Very high cycle fatigue for single phase ductile materials: Comparison between α-iron, copper and α-brass polycrystals

Véronique Favier, Antoine Blanche, Chong Wang, Ngoc Lam Phung, Nicolas Ranc, Danièle Wagner, Claude Bathias, André Chrysochoos, Hael Mughrabi

Very high cycle fatigue for single phase ductile materials: Comparison between α-iron, copper and α-brass polycrystals

Véronique Favier [a,*], Antoine Blanche [a,b], Chong Wang [c], Ngoc Lam Phung [a], Nicolas Ranc [a], Danièle Wagner [c], Claude Bathias [c,1], André Chrysochoos [b], Haël Mughrabi [d]

[a] Arts et Métiers ParisTech, CNRS PIMM, 75013 Paris, France
[b] Montpellier University, CNRS LMGC, 34095 Montpellier, France
[c] Paris Ouest Nanterre University, LEME EA 4416, 92410 Ville d'Avray, France
[d] Erlangen-Nürnberg University, Germany

Keywords:
Self-heating
Dissipated energy
Persistent slip bands
Crack initiation
Microstructure

A B S T R A C T

In this paper, the main results obtained in the framework of a National French Agency project called DISFAT, standing for "Dissipation in Fatigue", are presented. The project was dedicated to the microplastic mechanisms leading to crack initiation in the case of ductile metals loaded in very high cycle fatigue. Fatigue tests were carried out at 20 kHz using an ultrasonic facility. In order to investigate the microplastic mechanisms, slip markings at the surface of the specimens were observed and the self-heating of the specimen during the tests was measured by thermography to deduce the dissipated energy. Polycrystalline copper, α-brass and α-iron were investigated. A good correlation was found between persistent slip bands and dissipated energy. The dissipated energy for the three materials was of the same order of magnitude but while α-iron reached a stable dissipative state, the dissipated energy in the case of copper and α-brass was found to continue to increase gradually with increasing numbers of cycles. That change in dissipated energy during cycling was consistent with the development of persistent slip bands. Both were discussed with regard to the materials.

1. Introduction

Nowadays, many components used in aircraft, automobile and railway industries are required to have a fatigue life exceeding 10^7 cycles, corresponding to the so-called "very high cycle fatigue regime" (VHCF or the gigacycle regime). Ultrasonic fatigue facilities with frequencies in the range of tens of kilohertz are capable of producing 10^{10} cycles in less than one week while it would take three years using conventional fatigue machine. Two systems exist in literature. In the first type of systems, the load is continuously applied during the test [1,2] while in the second type, the load is applied discontinuously by blocks of cycles (pulse and pause modes) to avoid self-heating [3]. In parallel, new data analysis methods were developed. These methods involved infrared imaging techniques and aimed at assessing the dissipated energy associated with the cyclic loading [4–8]. In contrast to conventional fatigue tests, detecting irreversible microstructural changes using cyclic stress–strain curve analysis is no more possible, at ultrasonic frequencies, at least with conventional measurement systems, since the macroscopic behavior is quasi-elastic. To cope with this problem, the thermal signature of the deformation mechanisms was used. Self-heating of metallic materials is often related to microplasticity, i.e. the glide of dislocations, and progressively, to damage development. However, temperature fields depend on the distribution of dissipative sources but also on the environment and specimen geometry. That is why dissipated energy fields reflecting intrinsically internal changes of the material were preferred despite the experimental difficulties to overcome. The French National Agency supported from 2009 to 2014 a research project, named DISFAT, dedicated to dissipation in the very high cycle fatigue regime. It is recalled that Professor Claude Bathias initiated French research in the VHCF domain. Since the 1980 s, he contributed to develop the ultrasonic fatigue device and advocated its wider use. His outstanding contributions in this field are internationally recognized. Professor Claude Bathias participated actively in the DISFAT project and all co-authors consider it an

* Corresponding author.
E-mail addresses: veronique.favier@ensam.eu (V. Favier), antoine.blanche@u-montpellier.fr (A. Blanche), wangchongscu@163.com (C. Wang), ngoclam250@yahoo.com (N.L. Phung), nicolas.ranc@ensam.eu (N. Ranc), daniele.wagner@u-paris10.fr (D. Wagner), andre.chrysochoos@umontpellier.fr (A. Chrysochoos), hael.mughrabi@ww.uni-erlangen.de (H. Mughrabi).
[1] Deceased author.

honor and a duty to dedicate this review to his memory. Indeed, the aim of this paper is to synthesize the method we developed to identify dissipation fields that occur during ultrasonic fatigue tests and to present the main results we obtained. In this paper, polycrystalline copper, α-brass and α-iron (which contains a low amount of carbon) were studied. The materials investigated are all single-phase ductile materials. However, while copper and α-brass have a face-centered cubic (fcc) crystal structure, α-iron is body-centered cubic (bcc). These materials are so-called type I materials [9], in which crack initiation occurs at the surface owing to accumulation of very small but irreversible slips over very large numbers of load cycles resulting in slip markings. Here, the term "irreversible" is associated with cyclic slip processes inducing permanent or irreversible microstructural changes in the material resulting in damaging notch-peak geometries at the surface. The aim of this paper is to investigate the qualitative correlation between the dissipated energy and the slip markings for the three materials of interest during fatigue tests conducted at 20 kHz using an ultrasonic device and to compare the material responses. Some results obtained on copper and α-iron have been published [10–15]. These results are summarized and completed in order to compare the fracture, thermal and microstructural responses in VHCF. The findings concerning α-brass are completely new.

2. Material and experimental procedure

2.1. Experimental setup

The fatigue specimens were cylindrical and flat hourglass shaped. The fatigue tests were carried out at 20 kHz using an ultrasonic fatigue device. The latter allows to produce very high number of cycles in a reasonable time. In addition, high frequency loading raises the intrinsic dissipation and so induces large temperature variations whose low frequency components are easily detectable even by standard thermal measurement devices.

The ultrasonic fatigue facility was composed of a piezoelectric transducer which converted an electrical signal into a displacement and a horn which amplified the vibration and transmitted it to a specimen screwed on the horn and free of stress at its bottom extremity [1–3] (Fig. 1). The convertor, the horn and the "elastic" specimen composed a dynamic system designed so that its free resonant frequency in the first longitudinal mode was 20 kHz. Using a laser extensometer, the relationship between the displacement amplitude at the horn edge and the input electrical signal was obtained. Assuming pure linear elastic behavior, the strain and stress distributions along the specimen were estimated by a one-dimensional calculation for both specimen geometries. The calculated strain amplitude was checked to match the experimental measurement obtained by strain gages. Fig. 2 presents the geometry and the stress amplitude distribution in copper specimens [11].

2.2. Materials

Commercial OFHC (oxygen-free) copper (99.95% purity) and α-brass were investigated. The α-brass material contained 15 wt% Zn and 85 wt% Cu. The polycrystalline materials were hot rolled and supplied by Griset Company. The thickness of the hot rolled plate was 14 mm. The specimens were taken from the center of the plate. The α-iron was drawn from Armco iron extruded bars or sheets. The carbon content was 80 wt. ppm. Electron Back Scattering Diffraction maps of the three materials are shown in Fig. 3. The mean grain size was about 30 μm for the copper and α-iron polycrystals and about 10 μm for α-brass. The copper and α-brass polycrystals contained many annealed twins. In order to relieve the residual stress without any change of microstructure, the copper

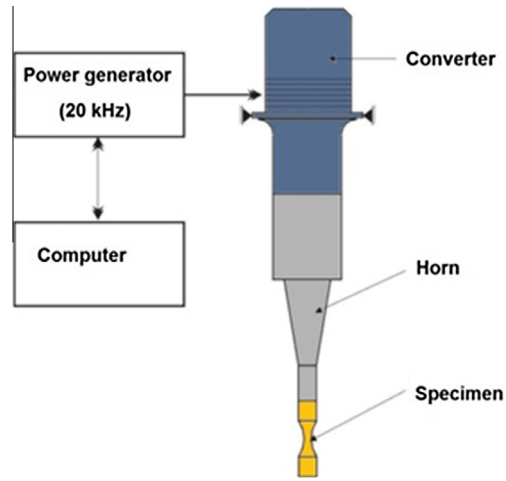

Fig. 1. Schematic representation of the piezoelectric system.

and α-brass specimens were heat treated by annealing for 60 min at 250 °C and 350 °C, respectively. Then, a procedure of mechanical and electrolytical polishing was applied to remove all hardened surface layers of the specimens. Before testing, the specimens were mirror polished without adding residual stresses. The Young moduli were taken as $E = 130$ GPa for copper and α-brass and $E = 210$ GPa for α-iron.

2.3. Experimental procedure

The S–N curve of the materials in the VHCF regime was first established. In order to avoid heating at high stress amplitudes, the specimens were cooled by a cold air gun during the test till rupture. Cylindrical specimens for copper and flat specimens for α-brass and α-iron were fatigued up to failure at various stress amplitudes. The stress ratio $R_\sigma = \sigma_{\max}/\sigma_{\min}$ was equal to −1. Scanning electron microscope (SEM) was used for fracture surface analysis. The inception and development of slip markings on the surface of the specimens were examined after interrupted tests at very low stress amplitudes using the flat specimens. This specimen geometry is suitable to observe the surface while assessing temperature fields with an infrared (IR) camera to derive the corresponding intrinsic dissipation patterns. One of the two flat faces of the specimen was black painted to carry out temperature measurements. The experiments were periodically interrupted after several specified numbers of cycles for surface observations.

3. Calorimetric analysis

3.1. Heat diffusion model

Ultrasonic fatigue tests involve dynamic mechanical processes. However, they are considered as quasi-static processes from a thermodynamic standpoint (see the statement of the local state axiom in [16]). Accordingly, the equilibrium material state can be described by a finite set of variables such as the absolute temperature T, the (small) strain tensor ε and a vector α of N internal state variables. Accounting for the local expressions of the first and second principles of Thermodynamics, and considering the Fourier heat conduction law, the local heat diffusion equation can be expressed as:

$$\rho C\dot{T} - \mathrm{div}(k\ \mathrm{grad}(T)) = d_1 + s_{the} + s_{thc} + r_{ext} \quad (1)$$

where ρ is the mass density, $C = -T\psi_{,TT}$ the specific heat, ψ the Helmholtz free energy, k the conduction tensor. The left hand side

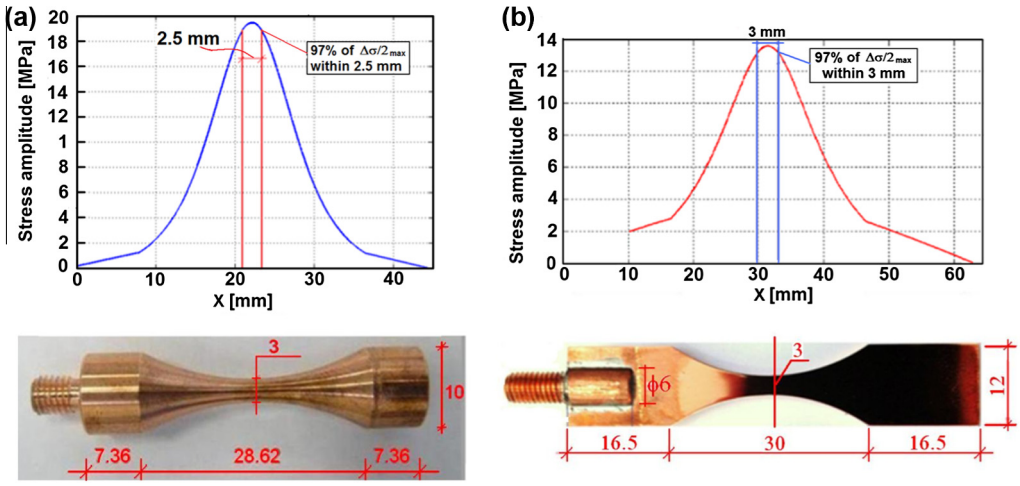

Fig. 2. Ultrasonic fatigue specimens and stress distributions along the specimen axis (a) cylindrical hourglass-shaped specimen and (b) flat hourglass-shaped specimen [11].

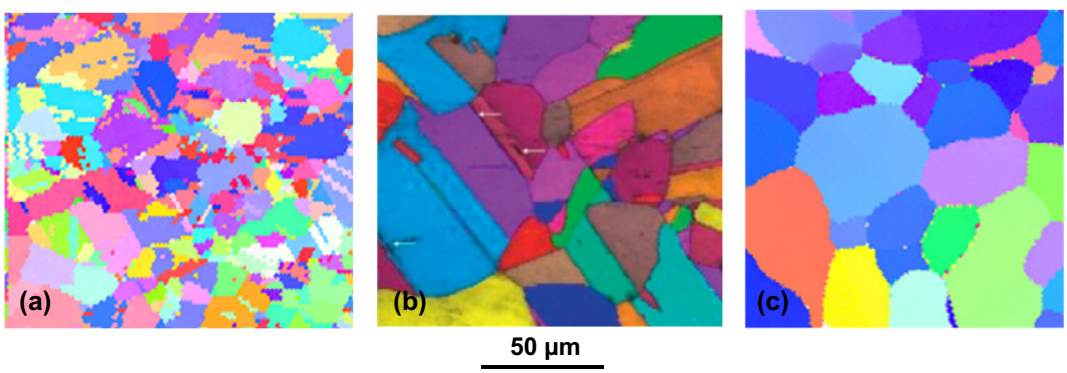

Fig. 3. Electron back scattering diffraction maps of polycrystalline materials: (a) α-brass, (b) copper (from [11]) and (c) α-iron (from [14]).

of this equation is a differential operator applied to T. The right hand side states different heat sources: the intrinsic dissipation $d_1 = \sigma : \dot{\varepsilon} - \rho\psi_{,\varepsilon} : \dot{\varepsilon} - \rho\psi_{,\alpha} \cdot \dot{\alpha}$, where σ is the Cauchy stress tensor, the thermoelastic source s_{the}, the other possible thermomechanical coupling sources s_{thc} (with $s_{the} + s_{thc} = \rho T\psi_{,T\varepsilon} : \dot{\varepsilon} + \rho T\psi_{,T\alpha} \cdot \dot{\alpha}$) and the external volume heat supply r_{ext}. We supposed that only dissipative and thermoelastic sources occurred during the material fatigue. We also considered that the mean thermoelastic source per cycle vanished. Finally, considering the maximum frame rate of the IR system (100 Hz) and the cyclic loading frequency (20 kHz), we only focused on the mean dissipated energy per cycle.

Following [4,5], hypotheses were considered to simplify the local heat diffusion equation:

- The isotropic conduction tensor k and the parameters ρ and C were constant, independent of the state variables.
- Thermoelastic effects were the only thermomechanical coupling factors considered hereafter.
- The thermal gradients varied slowly during the tests as compared to the characteristic cyclic loading time because of the thermal inertia. Besides, for such periodic loading, the mean velocity field was null over a cycle. As a result, the convective terms of the total time derivative of the temperature were neglected.
- The external heat supply was time-independent. The equilibrium temperature field T_0 fulfilled $-k\Delta T_0 = r_{ext}$. The temperature changes were expressed $\theta = T - T_0$.

Considering these hypotheses, the local 3D heat diffusion equation was rewritten into the simpler following form:

$$\rho C \frac{\partial \theta}{\partial t} - k\Delta\theta = d_1 + s_{the} \tag{2}$$

For thin flat specimens, it was shown that the mean temperature over the sample thickness $\bar{\theta}(t,x,y)$ remained close to the corresponding surface temperature $\theta_{IR}(t,x,y)$ given by the IR camera. An averaged heat diffusion equation over the sample thickness was then advantageously considered. Moreover, in the VHCF domain, the loading frequency (20 kHz), the maximum frame rate of the IR camera (100 Hz) and the considered stress ranges made the thermoelastic sources out of reach. During the VHCF tests, the temperature oscillations induced by the thermoelastic effects were not detected and only the mean dissipated energy per cycle could be derived from the discrete, noisy thermal data. The reader interesting in this tricky metrological and image processing problems can refer to [5] and more recently to [10,17].

3.2. Distributions of dissipated energy per cycle

Integrated over n loading cycles, the 2D heat diffusion model was finally formulated as:

$$\frac{1}{n}\int_t^{t+n/f_L} \rho C\left(\frac{\partial\bar{\theta}}{\partial t} + \frac{\bar{\theta}}{\tau^{2D}}\right) - k\left(\frac{\partial^2\bar{\theta}}{\partial x^2} + \frac{\partial^2\bar{\theta}}{\partial y^2}\right)dt = \overline{W}_d(t,x,y) \tag{3}$$

where f_L is the loading frequency; $\bar{\theta}(t,x,y)$ and $\overline{W}_d(t,x,y)$ respectively represented the depth-wise average distributions of the temperature variations and dissipated energy per cycle. The time constant $\tau^{2D} = \frac{\rho C e}{2h}$ characterized perpendicular heat exchanges

between the front and back specimen faces and the surroundings, where h and e were the heat exchange coefficient and the sample thickness, respectively. The construction of the heat source distribution via Eq. (3) required the evaluation of partial derivative operators applied to noisy digital signals. To compute reliable estimates of heat sources, it was then necessary to reduce the noise amplitude without modifying the spatial and temporal thermal gradients. Among several possible methods, a special local least-squares fitting of the thermal signal was considered in this work. The local fitting function $\bar{\theta}_{fit}$ of the temperature charts was chosen as:

$$\bar{\theta}_{fit}(t,x,y) = p_1(x,y)t + p_2(x,y) \tag{4}$$

where the functions $p_i(x, y)$, $i = 1,2$, are 2nd order polynomials in x and y. These polynomials enabled us to account for the possible spatial heterogeneity of the source patterns. A linear function of time was chosen, assuming that the dissipative fatigue mechanisms slowly progressed and could be piece-wise linearized, throughout the short time intervals corresponding to each approximation zone.

The 2D fields of dissipated energy per cycle were computed over rectangle $L \times l$ centered on the sample gage part. In practice, L was about 6 mm and l about 2 mm. Longitudinal profiles of mean dissipated energy per cycle were directly derived averaging the 2D dissipated energy fields in the width direction.

$$\overline{\overline{W}}_d(t,x) = \frac{1}{l}\int_{-l/2}^{l/2} (\overline{W}_d(t,x,y))dy \tag{5}$$

The mean dissipated energy $\langle \overline{W}_d \rangle(t)$ averaged over the sample gage part was simply computed as:

$$\langle \overline{W}_d \rangle(t) = \frac{1}{L \times l}\int_{-L/2}^{L/2}\int_{-l/2}^{l/2} (\overline{W}_d(t,x,y))dydx \tag{6}$$

In the following, the dissipative deformation mechanisms of the materials under investigations were discussed in terms of (i) $\overline{W}_d$, fields of dissipated energy per cycle (cf. Eq. (3)), (ii) $\overline{\overline{W}}_d$, profiles of dissipated energy per cycle (cf. Eq. (5)) and (iii) $\langle \overline{W}_d \rangle$, mean dissipated averaged over the sample gage part (cf. Eq. (6)).

4. Results

4.1. S–N curves

The S–N curves of the three materials obtained after cooled fatigue tests are shown in Fig. 4. Specimens which did not fail (runnouts) are marked with arrows. The fatigue strength was found to decrease by 10 MPa per decade above 2×10^7 cycles for the three materials. No failure was observed at $\Delta\sigma/2 = 91.2$ MPa up to 5.4×10^9 cycles for copper and at $\Delta\sigma/2 = 190$ MPa up to 6.5×10^9 cycles for α-iron, for which the tests were stopped. All the α-brass specimens were broken, and no fatigue test was carried out for $\Delta\sigma/2$ below 164 MPa and number of cycles in excess of 1.5×10^9 cycles. Results obtained for copper were consistent with Stanzl-Tschegg et al.'s experimental results obtained on polycrystalline copper of similar purity [18,19]. For the three materials, no horizontal asymptote that can be related to a fatigue limit was detected up to 10^{10} cycles. However, a reference endurance limit σ_D, also called fatigue limit in the following, was considered for the three materials for the need of material comparisons. It was estimated at the value of the fatigue strength at 10^9 cycles from the S–N curves obtained with a cooling system. σ_D was found equal to 90 MPa for copper, 164 MPa for α-brass and 190 MPa for α-iron specimens, respectively.

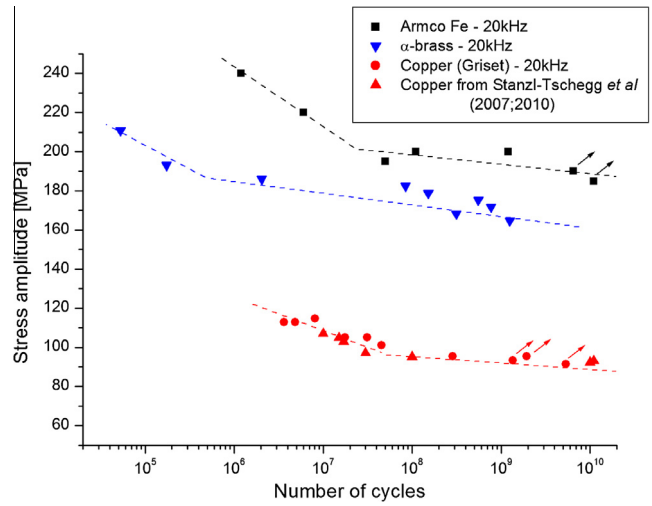

Fig. 4. S–N curves for α-iron, α-brass and copper specimens fatigue loaded at 20 kHz. Comparison with Stanzl-Tschegg et al.'s results obtained for copper [18,19]. Specimens which did not fail (runnouts) are marked with arrows.

4.2. Fractographic observations

Fracture surface observations showed that surface failure occurred for the three materials as commonly observed for type I materials [9,20,21]. When slip markings were observed on the three materials, it was checked whether they were persistent slip bands (PSBs). For this purpose, the fatigue test was interrupted, the surface was electropolished, and fatigue was resumed. The slip bands were regarded as persistent slip bands, if they reappeared at the same sites. For copper and α-iron specimens, microcracks were observed at grain boundaries located between a grain with PSBs and another grain without PSBs in the vicinity of the grain boundary (Figs. 5 and 6a). For copper specimens, the VHCF crack initiated at such grain boundaries while for α-iron specimens, PSBs crossing grains were found to be additional crack initiation locations (Fig. 6b). For α-brass, the crack initiation location was not clearly identified in the studied specimens.

4.3. Self-heating

Fig. 7 exhibits the evolution of the temperature increase for copper, α-brass and α-iron specimens during fatigue tests without cooling. The higher the stress range, the higher the self-heating. For the three materials, the stress amplitude ranges corresponded approximately to stress amplitudes ranging from 42% to 66% of material fatigue endurance σ_D. Table 1 specifies the stress amplitude ranges for the three materials. The self-heating was found less than 20 °C for copper specimens loaded between 41 MPa and 56 MPa, less than 90 °C for α-brass specimens loaded between 72 MPa and 100 MPa and less than 80 °C for α-iron specimens loaded between 80 MPa and 125 MPa. In order to assess the evolution of self-heating with increasing numbers of cycles, the self-heating was normalized to a reference self-heating temperature θ_{Ref}, arbitrarily chosen as the self-heating obtained at a stress amplitude of about 60% of the endurance limit σ_D, namely $\theta_{Ref} = 10$ °C for copper, $\theta_{Ref} = 60$ °C for α-brass and $\theta_{Ref} = 55$ °C for α-iron. This normalization allowed having similar scales for the three materials (Fig. 7). The temperature had a sharp increase at the beginning of the test, allowed by quasi-adiabatic conditions. Then, the self-heating gradually increased up to 10^6 cycles for the three materials. It should be noted that the scale for the number of cycles is different for the three graphs of Fig. 7. In the case of copper, 10^8 cycles were reached (Fig. 7a), in the case of α-iron,

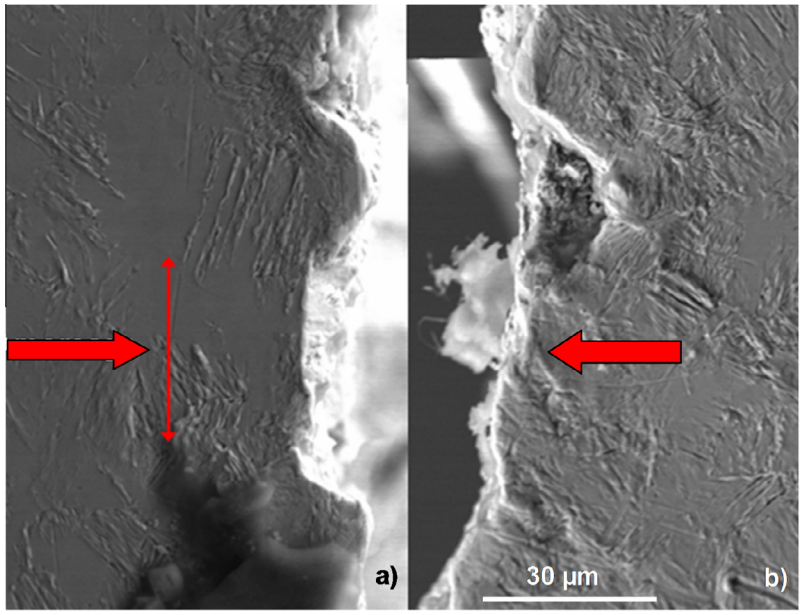

Fig. 5. Fractographic observations made on a copper specimen loaded at a stress amplitude of 105 MPa; $N = 3.1 \times 10^7$, specimen surface normal to the fracture [11]: (a) left side, zone free of slip bands, (b) right side, zone marked with persistent slip bands.

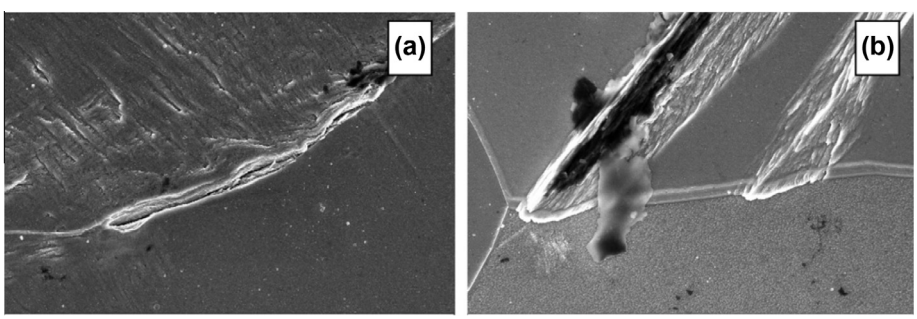

Fig. 6. Specimen surface observations for an α-iron specimen loaded at a stress amplitude of 120 MPa; $N = 1 \times 10^8$ [14]: (a) microcrack along grain boundary, (b) microcrack in persistent slip bands.

10^7 cycles (Fig. 7d) and only 10^6 cycles in the case of α-brass (Fig. 7b and c). However, a clear difference in thermal response was observed for copper and α-iron between 10^6 and 10^7 cycles. No change in temperature was experimentally measured at low stress amplitudes (80, 90 and 100 MPa) for α-iron. A thermal steady-state was thus reached after 5×10^6 cycles. For higher stress amplitudes (110 and 125 MPa), the self-heating change remained very slight. In contrast, in the case of copper, the temperature always increased with increasing numbers of cycles and no steady state was found for all the studied stress amplitudes even up to 10^8 cycles. In the case of α-brass, a test at a stress amplitude of 75 MPa was carried out up to 10^7 cycles (Fig. 7c). The self-heating was found to be constant after about 6×10^7 cycles. This thermal response is thus different from that of copper but similar to that of α-iron one for the same normalized stress amplitude (~45%). For the three materials, the initiation of fracture led to a final sharp temperature increase. It should be noted that self-heating was detected for all the stress amplitudes studied.

4.4. Dissipated energy per cycle of materials during fatigue tests and correlation with slip markings and cracks

4.4.1. Map of dissipated energy per cycle $\overline{W}_d$

Fig. 8a exhibits the 2D temperature map of an α-iron specimen loaded at a stress amplitude of 120 MPa up to 5×10^6 cycles without cooling system. The 2D dissipated energy $\overline{W}_d$ map over the black rectangle was derived from the temperature map (Fig. 8b). The dissipated energy field was clearly inhomogeneous and displayed a not very well defined zone for which it was the highest. This zone was roughly consistent with the zone for which the stress amplitude gradient profile was maximum: the stress amplitude was the highest in the center of the specimen (represented by the black dotted line in Fig. 8b) and was almost constant 1.5 mm apart from the center (see also Fig. 2). However, the place corresponding to the highest dissipated energy (red[2] in Fig. 8b) was thinner. Thus, the dissipated energy profile was more concentrated than the stress amplitude profile. It was also slightly shifted with regard to the center of the specimen. In addition some small spots of dissipated energy (green-yellow zones in Fig. 8b) occurred further away from the specimen center. The dissipated energy gradients remained small in the width direction of the specimen, justifying the use of profiles of dissipated energy per cycle.

4.4.2. Profile of dissipated energy per cycle $\overline{\overline{W}}_d$

Fig. 9 displays the dissipated energy profile $\overline{\overline{W}}_d$ along the specimen axis of copper loaded at a stress amplitude of 72 MPa after

[2] For interpretation of color in Fig. 8, the reader is referred to the web version of this article.

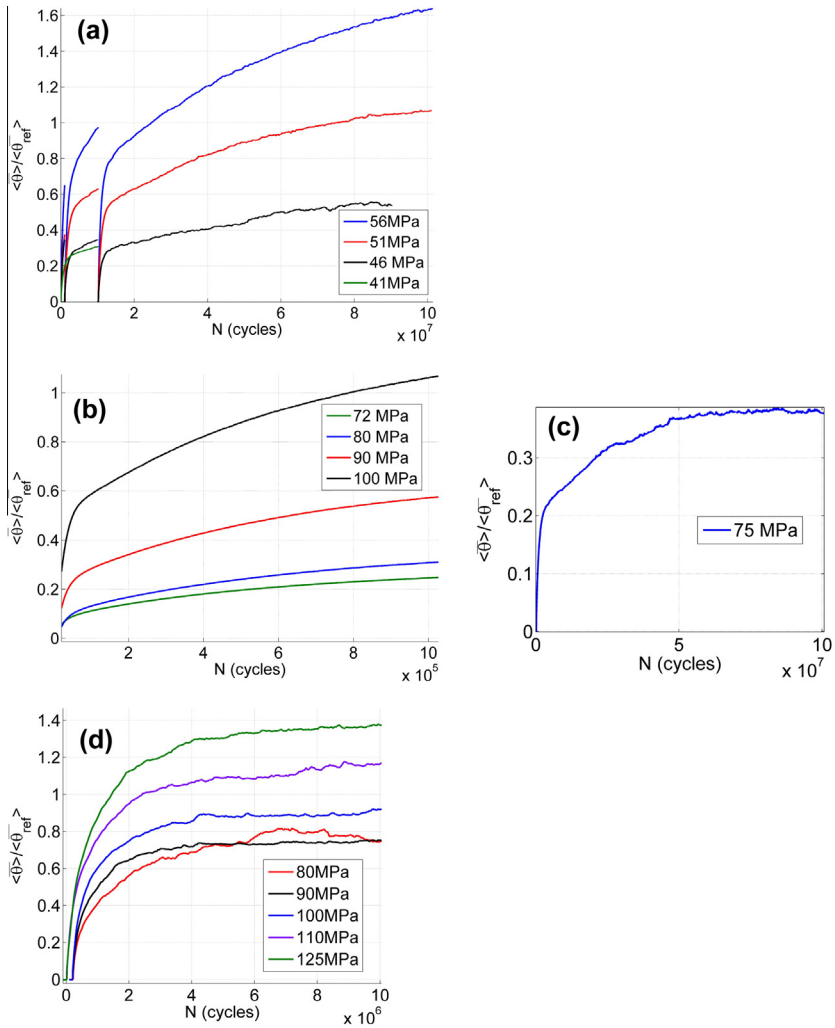

Fig. 7. Self-heating evolution as a function of number of cycles and for various stress amplitudes: (a) copper, (b) and (c) α-brass, (d) α-iron.

Table 1
Stress amplitudes and stress amplitudes normalized with respect to the fatigue strength at 10^9 cycles, for the copper, α-brass and α-iron specimens.

Copper (σ_D = 90 MPa)		α-brass (σ_D = 164 MPa)		α-iron (σ_D = 190 MPa)	
$\Delta\sigma/2$ (MPa)	$\Delta\sigma/2/\sigma_D$	$\Delta\sigma/2$ (MPa)	$\Delta\sigma/2/\sigma_D$	$\Delta\sigma/2$ (MPa)	$\Delta\sigma/2/\sigma_D$
42	45.6%	72	43.9%	80	42.1%
46	21.1%	80	48.8%	90	47.4%
51	56.7%	90	54.9%	100	52.5%
56	62.2%	100	60.9%	110	57.9%
				125	65.8%

10^7 cycles without cooling system. Also in the case of α-iron, the dissipated energy was not highest at the specimen center but at the place, where most slip markings were found. Fig. 10 displays the dissipated energy profile along the specimen axis at the beginning, in the middle and at the end (rupture) of a fatigue test carried out on α-iron without cooling system. The dissipated energy globally increased with increasing numbers of cycles. It should be noted that the dissipated energy maximum moved slightly along the specimen axis during cycling. As the dissipated energy zone developed, it became more and more concentrated and was finally located in the zone in which the final rupture took place. In summary, for such single-phase ductile materials, the dissipation energy field was related to the overall stress amplitude field but depended also on the local heterogeneities within the material leading to a non-perfect match between stress amplitude and dissipated energy profiles. The zone of highest plastic activity, identified as the zone having the largest number of slip bands, corresponded to the zone of highest dissipated energy. The dissipative mechanisms of plasticity and crack initiation presumably localized during cycling, leading to strong localization of dissipated energy and the final rupture of the specimen.

4.4.3. Mean dissipated energy per cycle $\langle \overline{W}_d \rangle$

4.4.3.1. Case of copper. The dissipated energy profiles $\overline{\overline{W}}_d$ were used to calculate the mean dissipated energy $\langle \overline{W}_d \rangle$ averaged over 6×2 mm^2 area at the specimen center (see 3.2). The mean dissipated energy in fatigued copper was plotted as a function of the number of cycles for four stress amplitudes ranging from 51% to 80% of σ_D (Fig. 11a). It should be noted that the number of cycles were plotted on a logarithmic scale which gave a concave upwards curve while on a linear scale, the curve was convex upwards. The tests carried out at stress amplitudes of 46, 51 and 56 MPa were interrupted at 10^6, 10^7 and 10^8 cycles to observe the surface of the specimens by scanning electron microscopy, as shown in Fig. 11b.

At a stress amplitude of 46 MPa, the mean dissipated energy increased slightly during cycling up to 10^8 cycles, as shown in the zoomed insert in Fig. 11a. However, no slip band was observed up to 10^8 cycles on the specimen surface (Fig. 11b). At a stress

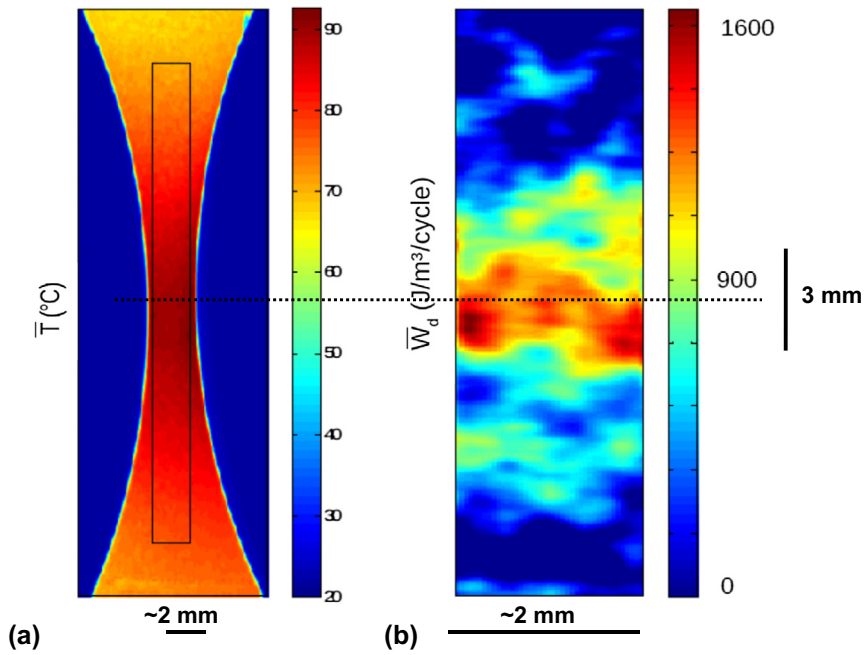

Fig. 8. Temperature and dissipated energy maps of an α-iron specimen loaded at a stress amplitude of 120 MPa, $N \cong 2.5 \times 106$ cycles, without cooling system: (a) temperature map, (b) dissipated energy map per cycle $\overline{W}_d$ derived from the temperature over a rectangle $L = 6$ mm × $l = 2$ mm centered on the sample gage part.

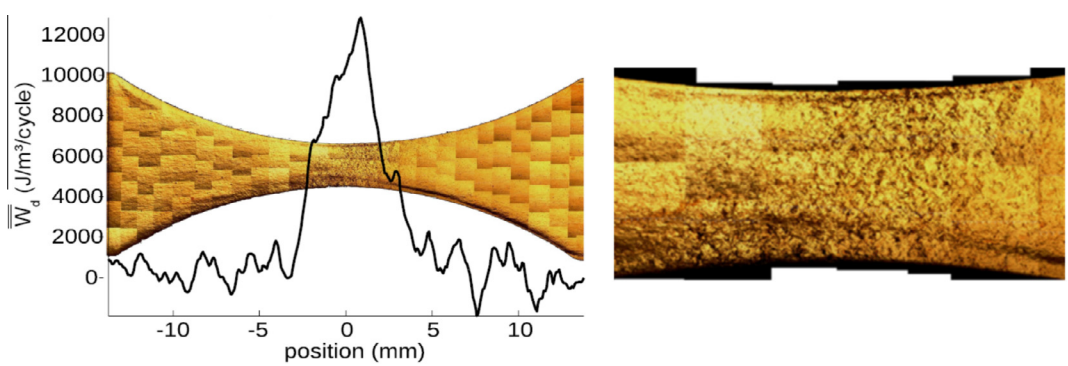

Fig. 9. Profile of dissipated energy per cycle $\overline{\overline{W}}_d$ along the specimen axis and optical micrographs of corresponding panorama of the surface of a copper specimen fatigued at $\Delta\sigma/2 = 72$ MPa for 10^7 cycles without cooling system. On the right: enlarged section of the middle of the gauge length of the specimen.

amplitude of 51 MPa, the mean dissipated energy again increased during cycling, and the change in dissipation was somewhat stronger than at a stress amplitude of 46 MPa. No slip band was observed at 10^7 cycles. However, straight, short and very fine slip bands were found after 10^8 cycles. The black stains in the micrograph in Fig. 11b corresponded to marks of black paint used on the opposite surface of the specimen in order to perform IR temperature measurements. At a stress amplitude of 56 MPa, a similar mean dissipated energy evolution curve was noted but the value of the mean dissipated energy value was higher than the value found at lower stress amplitudes. Slip bands were detected at 10^7 cycles and clearly grew and multiplied with increasing numbers of cycles. At a stress amplitude of 72 MPa, the mean dissipated energy was found to be much higher and increased steeply during cycling. Many straight slip bands were observed. They were clearly longer and wider than the slip bands observed at the stress amplitude of 51 MPa. All the results obtained on fatigued copper demonstrated that a clear relationship existed between the dissipated energy and the slip bands on the specimen surface. The highest dissipated energy location corresponded to the zone having the largest number of slip bands and the change in dissipation was accompanied by a change in the quantity of slip bands. The copper specimens were found to dissipate energy even, when no slip band was observed on the specimen surface. A significant self-heating of about 1.5 °C was found for a stress amplitude as low as 15 MPa but it was too low to assess reliable intrinsic dissipation from Eq. (3).

4.4.3.2. Case of α-iron. Fig. 12a exhibits the evolution of the mean self-heating during cycling for an α-iron specimen at a stress amplitude of 120 MPa, corresponding to about 63% of σ_D. As already mentioned in Section 4.3, a thermal quasi-steady-state was reached after a large number of cycles. The mean dissipated energy was also found to be nearly constant after a large number of cycles. Fig. 13 shows optical micrographs of the surface of an α-iron specimen fatigued at a stress amplitude of 110 MPa (58% of σ_D). The test was interrupted at 10^8 and 2×10^9 cycles for observation of the surface. Some persistent slip markings were detected. They occurred in very few grains and covered the whole grain surfaces. The neighbor grains did not exhibit any slip markings. Persistent slip markings did not progress from 10^8 cycles and 2×10^9 cycles, but broadened very slightly [15]. These results on

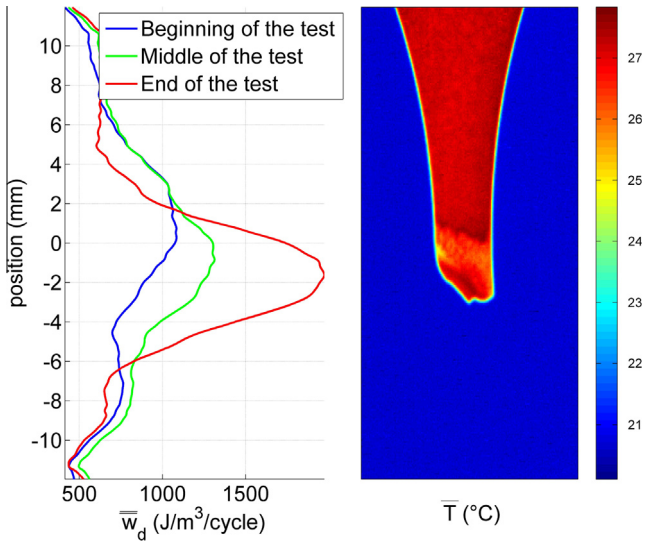

Fig. 10. Profile of dissipated energy per cycle $\overline{\overline{W}}_d$ along the axis of a fatigued α-iron specimen at the beginning, in the middle and at the end (rupture) of the test and corresponding infrared thermography map of the specimen at rupture. The stress amplitude was 120 MPa and no cooling system was used during cycling. The temperature scale is given in °C.

α-iron demonstrated that, in contrast to the observations on fatigued copper and for similar stress amplitudes with regard to σ_D, the dissipated energy strongly increased when the fatigue test started but then did not change any more after large number of cycles. The constancy of the dissipated energy is consistent with the fact that the slip markings did not seem to change much during further fatigue of α-iron.

4.4.3.3. Case of α-brass. Fig. 14a shows the evolution of the mean self-heating during cycling deformation of an α-brass specimen at a stress amplitude of 75 MPa (45% of σ_D). It corresponds to the earlier Fig. 7c, with the original ordinate scale (relative temperature) replaced by absolute temperature. As in the case of α-iron, a thermal quasi-steady-state was reached after a large number of cycles. However, as opposed to the case of α-iron, the mean dissipated energy $\langle \overline{W}_d \rangle$ was found to increase during cycling deformation (Fig. 14b). The dissipative behavior of α-bass is thus similar to that of copper. Fig. 15 shows micrographs of the surface of an α-brass specimen after 10^6 cycles at a stress amplitude of 134 MPa (82% of σ_D). The PSBs are straight and long. Some are along twin boundaries and others cross the grains. They are inclined at an angle of ∼45° from the loading axis. Some PSBs were transmitted through a grain or twin boundary (indicated by dotted line arrows). At some places (indicated by (1)), the transmission occurred through two boundaries and the slip bands in the first and third grains are parallel, suggesting that the second grain, in the middle, is a twin embedded into the matrix. As far as slip band evolution is concerned, the slip bands were found to grow in length and in width with increasing numbers of cycles in good agreement with the dissipative response.

The numbers of cycles needed to form the early persistent slip markings as a function of the stress amplitude are shown in Fig. 16. For the sake of comparison, the data in the case of copper were added. They were published in a previous paper [11]. At a given stress amplitude, the test was regularly interrupted to observe the slip markings on the specimen surface. In Fig. 16, the experimental data indicate the last observation before slip markings appeared and the next observation when the early slip markings were first detected using SEM. Similarly to copper, the stress amplitude decreased linearly with the logarithm of increasing numbers of cycles necessary to form the early slip markings. No slip marking was observed in the region below the data. Above them, persistent slip bands were present at the surface of the specimens. In the case of α-brass, no slip band was observed at 10^{10} -cycles below 62 MPa. In the case of copper, no slip band was observed at 2×10^9 cycles below 41 MPa [11] and at 10^{10} cycles below 34 MPa [18]. The decreasing slope of the early PSbs curve was slightly stronger in the case of α-brass than in the case of copper.

4.4.3.4. Mean dissipated energy per cycle $\langle \overline{W}_d \rangle$-stress amplitude curve for the three materials. Fig. 17a shows the mean dissipated energy per cycle $\langle \overline{W}_d \rangle$ at 10^6 cycles as a function of the stress amplitude normalized by the fatigue limit σ_D for the three materials. The mean dissipated energy for the three materials changed slightly with stress amplitudes when the latter were low but increased steeply above a specific range of stress amplitudes. The dissipated energy for α-brass was found to increase steeply for lower stress amplitudes normalized with respect to the fatigue limit than for copper and α-iron. It should be noted that, in the case of α-iron, only the dissipated energy corresponding to the low stress amplitude range was measured. Fig. 17b exhibits the same results, but the stress amplitudes were normalized with respect to the ultimate tensile stress UTS (232 MPa for copper, 306 MPa for α-brass and 400 MPa for α-iron) instead of the fatigue limit. The difference between the curves is clearly reduced showing that the dissipated energy is very similar for the three materials.

5. Discussion

5.1. Morphology, location of persistent slip bands

Fig. 11b shows a micrograph of the surface of a copper specimen observed after 10^7 fatigue loadings at a stress amplitude of about 34% of the ultimate tensile stress (72 MPa). Fig. 13a shows the same for an α-iron specimen after 10^8 cycles and for a similar stress amplitude range, normalized with respect to the ultimate tensile stress. Fig. 15 exhibits the same for an α-brass specimen after 10^6 cycles and a similar normalized stress amplitude range. In the case of copper and α-brass specimens, the slip bands were straight and long and crossed the grains. They gathered in families of about ten parallel slip markings and occurred in many grains. Both materials contained annealed twins. Phung et al. [11,12] demonstrated that twin boundaries inclined at an angle of ∼45° were preferential sites for appearance of early slip markings for copper cyclically loaded at very low stress amplitudes because of strong stress concentrations due to anisotropic elasticity and the existence of well-oriented slip planes parallel to the twin boundary plane. At higher stress amplitudes such as 34% of the ultimate tensile stress, local stresses were high enough to generate slip bands in the whole well-oriented grain. These slip bands were associated with the persistent slip bands commonly observed in the low and high cycle fatigue regimes [22]. In most of the cases, PSBs did not transmit through grain boundaries. However, Figs. 11b and 15 revealed that some PSBs were transmitted through a grain or twin boundary (indicated by dotted line arrows). The PSB transmission process was found more prevalent for α-brass than that of copper. The stress concentrations at twin or grain boundaries are expected to be stronger for α-brass than for copper. Indeed, the anisotropy coefficient is much higher for α-brass than for copper (8 versus 3.3). As a result, the strain incompatibilities were stronger. Besides, the stacking fault energy of α-brass is lower (<10 mJ/m^2 with respect to about 40 mJ/m^2 for copper [23]). As a result, cross slip events occured more rarely which favored dislocation pile-ups.

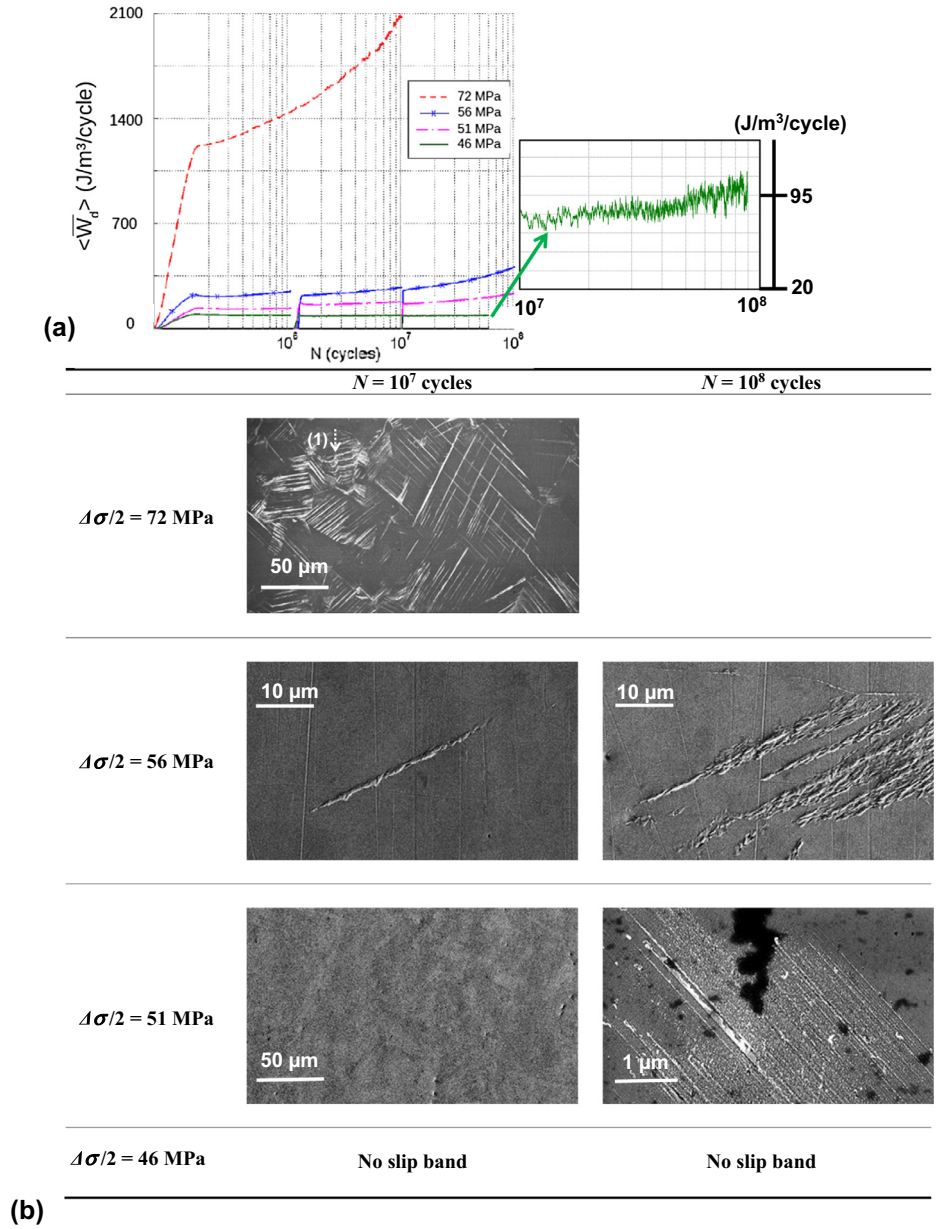

Fig. 11. Evolution of the mean dissipated energy $\langle \overline{W}_d \rangle$ in fatigued copper as a function of the number of cycles (logarithmic scale). No cooling system was used: (a) evolution for various stress amplitudes, with zoomed example of recording at 46 MPa. (b) Scanning electron micrographs of the surface of the specimens after interruption of the fatigue tests after 10^7 and 10^8 cycles. The loading axis is horizontal. The white dotted line arrow on the micrograph corresponding to 72 MPa indicates slip bands transmitted through twin boundaries. The "(1)" indicates that the transmission occurred through two boundaries revealing the presence of a twin and two twin boundaries.

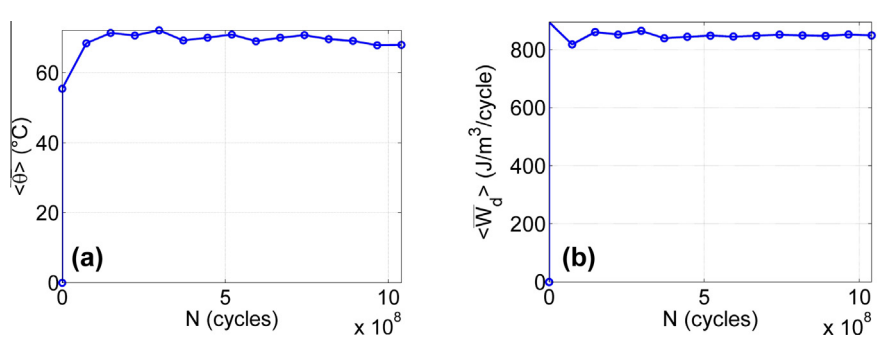

Fig. 12. Evolution of the self-heating and mean dissipated energy in α-iron fatigued at a stress amplitude of 120 MPa as a function of the number of cycles up to 10^9 cycles: (a) self-heating, (b) mean dissipated energy per cycle $\langle \overline{W}_d \rangle$.

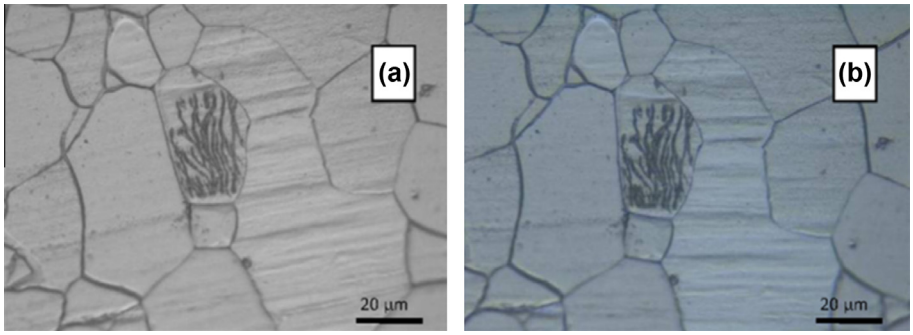

Fig. 13. Optical micrographs of the surface of a specimen of α-iron, fatigue loading at a stress amplitude of 110 MPa (about 60% of σ_D): (a) 10^8 cycles, (b) 2×10^9 cycles.

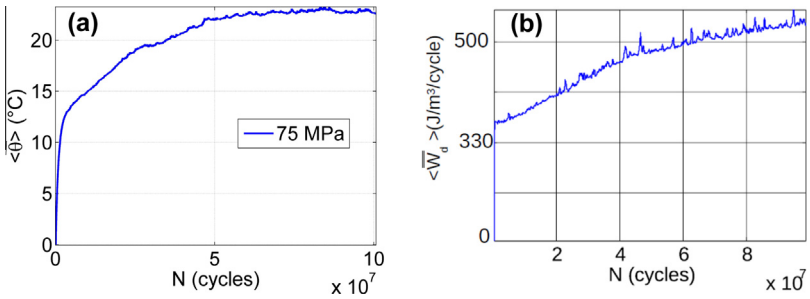

Fig. 14. Evolution of the self-heating and the mean dissipated energy in α-brass fatigued at a stress amplitude of 75 MPa as a function of the number of cycles up to 10^8 cycles, (a) self-heating (it corresponds to the earlier Fig. 7c), with the original ordinate scale (relative temperature) replaced by absolute temperature). (b) Mean dissipated energy per cycle $\langle \overline{W}_d \rangle$.

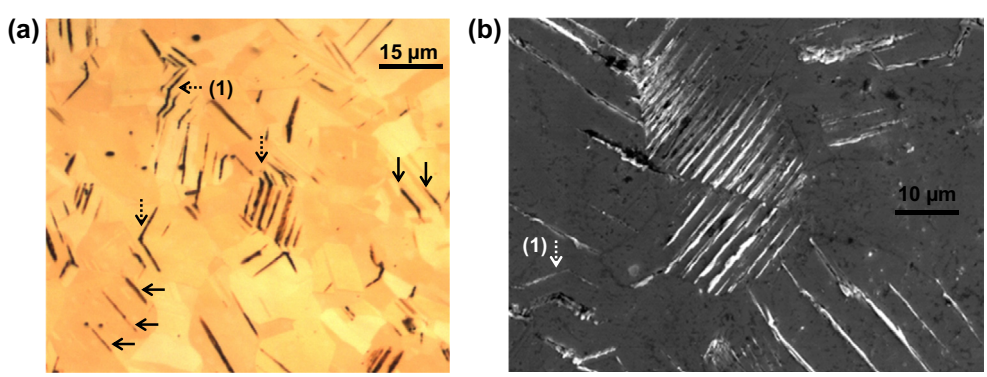

Fig. 15. Micrograph of the surface of an α-brass specimen observed after 10^6 cycles of fatigue loading at a stress amplitude of 134 MPa (82% of σ_D and about 44% of the ultimate tensile stress). The loading axis is horizontal: (a) optical micrograph, the black full line arrows indicate twin boundaries and the black dotted lines arrow indicate slip bands transmitted through grain or twin boundaries. (b) Scanning electron micrograph.

The higher stress concentrations, due to both anisotropy coefficient and dislocation pile-ups, at twin or grain boundaries, promoted the activation of plasticity and slip band emergence in the neighbor grain more frequently in α-brass than in copper.

While the PSBs in copper and α-brass were straight, the PSBs in α-iron were wavy. Similar wavy persistent slip markings were observed by Mughrabi et al. [24] on single crystals of α-iron containing 30 wt. ppm carbon after cyclic loading. More recently, similar wavy PSBs, crossing one grain, were observed by Munier [25] on a high-strength-low-alloy steel containing a ferritic phase like α-iron, after fatigue at 30 Hz. The presence of wavy slip lines reveals that cross slip occurred easily [26]. The 20 kHz fatigue tests induced strain rates ranging between 10 s^{-1} and 100 s^{-1} according to the prescribed displacement. As a result, the transition temperature between the thermally activated regime (low-temperature mode of deformation of bcc metals) and the athermal regime raised above room temperature [24] so that "low-temperature" behavior prevailed at room temperature. In the present case, this is considered to be also true even if self-heating occurred (see end of Section 5.2). In pure iron, screw dislocations are almost immobile at room temperature, while edge dislocations move quite easily. The present α-iron was not pure and contained 80 wt. ppm carbon. In the presence of the interstitial carbon solute atoms, the edge dislocations are slowed down so that the mobilities of edge and screw dislocations become comparable like in fcc metals [27]. Once screw dislocations in bcc metals are mobile, they can cross slip readily. Moreover, the frequency of cross slip of screw dislocations is favored by the fact that the ⟨1 1 1⟩ slip directions are contained in each of the {1 1 0}, {1 1 2} and {1 2 3} slip planes, all of which thus are possible cross slip planes. The number of possible cross slip planes is thus higher for bcc than fcc metals (only two in the latter case). As a result, the slip is wavy and the local slip irreversibility in the wavy PSBs increases. That explains why the PSBs were wavy in the case of α-iron. The PSBs were found

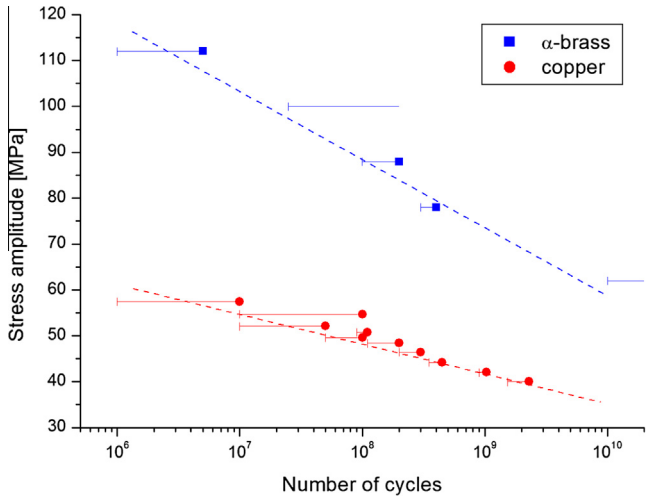

Fig. 16. Stress amplitude needed to form the early slip markings as a function of the number of cycles in the case of copper and α-brass. At a given stress amplitude, the vertical bars indicate the last observation before slip markings appeared and the squares and the circles represent the subsequent observation (when it existed) when the early slip markings were detected using SEM.

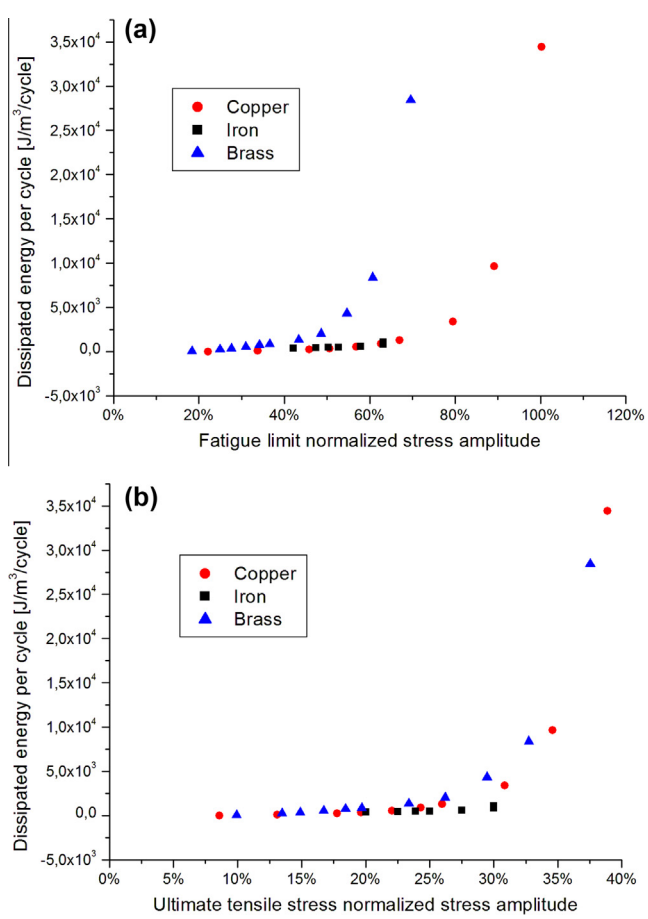

Fig. 17. Evolution of the mean dissipated energy per cycle $\langle \overline{W}_d \rangle$ at 10^6 cycles for copper, α-brass and α-iron as a function of stress amplitudes normalized with respect to (a) the fatigue limit σ_D or (b) the ultimate tensile stress.

only within a grain. α-Iron does not contain any twins. Its anisotropy elastic coefficient is 2.4 [28] and thus lower than for copper and α-brass. As a result, the appearance of the slip markings was controlled more by the grain orientation than by neighboring effects and misorientations at grain boundaries. Therefore, PSBs crossed the grains which were most favorably oriented for plastic deformation.

5.2. Mean dissipated energy per cycle $\langle \overline{W}_d \rangle$ during cycling

In high cycle fatigue tests, a thermal steady-state occurs sometimes. In such conditions, the intrinsic dissipation is balanced by the heat losses, and the dissipated energy per cycle can be considered as a constant induced by a constant population of microdefects. In the case of very high cycle fatigue tests, for stress amplitudes ranging from 20% to 30% of the UTS, a growing dissipation during cycling was observed in the case of copper and α-brass. Thus, the microstructural state progressed cycle by cycle that was assessed *via* a permanent evolution of the slip bands on the surface of the specimens. The development of PSBs on the surface of the specimens with increasing numbers of cycles indicates that the macroscopic plastic strain amplitude increased. As ultrasonic fatigue tests were total strain-controlled tests, the macroscopic stress amplitude was deduced to decrease. The plastic strain amplitude increase is related to the rearrangement of dislocations leading to highly strain accommodating within the grains (mostly in PSBs). From a thermodynamic standpoint, considering that, ideally, the fatigue limit is associated with no change of dissipated and stored energy from one cycle to another [10], no stress amplitude between 20% and 30% of UTS (corresponding to 45% up to 80% of σ_D) can be considered as a true fatigue limit. It seems that "there is no infinite fatigue life" as claimed Claude Bathias in [29]. Studying evolution of the dissipated energy beyond 10^9–10^{10} cycles would be necessary to conclude on the existence of a fatigue limit. Comparing Figs. 4 and 16 show that, for a specified number of cycles, the stress amplitude required to break the specimen was about twice larger than the stress amplitude needed to form the early PSBs for both fcc metals. In the case of copper, Stanzl-Tschegg et al. [19] observed many short intergranular and transgranular cracks below σ_D (90 MPa). However, they demonstrated that the associated stress intensity factors were lower than the stress intensity threshold necessary for crack growth. Consequently, the short cracks did not propagate. Fatigue failure required to increase the stress amplitudes. The transition between crack initiation to propagation still needs clarification.

In contrast to the case of copper, the evolution of the dissipated energy reached a constant value in the case of α-iron loaded at 120 MPa (30% of UTS) up to 10^8 cycles. Considering the low-temperature deformation mode for the studied α-iron, cyclic hardening and microstructural changes are almost negligible for plastic strain magnitude below 5×10^{-4} [24]. The screw dislocations are nearly immobile. The edge dislocations move to-and-fro in a non-hardening quasi reversible manner. That motion leads to a constant dissipated energy and no change in stored energy with increasing numbers of cycles. This mechanism could occur in most of the grains of the α-iron studied here. However, the rare grains exhibiting wavy slip bands revealed the presence of cross slip of screw dislocations as discussed in Section 5.1. In the case of α-iron single crystal, cyclically loaded at controlled plastic strain amplitude of $\sim 10^{-4}$ and plastic strain rate below 10^{-2} s^{-1}, Mughrabi et al. [30] observed constant stress amplitude (no hardening) and minor increase of dislocation density with increasing numbers of cycles. They concluded that the negligible cyclic hardening was the consequence of strongly impeded dislocation multiplication. At larger plastic strain amplitudes ($\sim 10^{-3}$), the multiplication of dislocations was easier leading to strain-hardening but which rapidly saturated because the multiplication is balanced by annihilation of screw dislocation which cross slips. In the present case, the macroscopic strain amplitudes varied between 2×10^{-4} and 6×10^{-4}. Thus, the macroscopic plastic strain is expected to be below

10^{-4}. As a result, the deformation was likely accommodated by the to-and-fro of edge dislocations occurring in most of the grains. Screw dislocations were certainly more mobile in the well-oriented grain for plasticity as discussed in Section 5.1. The value of the dissipated energy of the two mechanisms is difficult to estimate. However, it is expected to remain quasi-constant with increasing numbers of cycles since no significant microstructural state changes are associated with these mechanisms. As a result, in the case of α-iron loaded between 80 and 120 MPa, after a transition regime of cycling, the macroscopic dissipated energy (considered as the spatial average of the microscopic dissipated energy) remained constant with increasing numbers of cycles. The microstructural state remained also nearly unchanged. No final fatigue failure is thus expected at very high number of fatigue suggesting that there is a fatigue limit in that case. It should be noted that the self-heating of the specimen (80 °C at 120 MPa) does not change the low-temperature mechanisms mentioned above. Indeed, Campbell and Fergusson [31] showed that for steels containing 0.12 wt% of carbon, so not so far form the present α-iron, the transition temperature was shifted to 130–400 °C for strain rate ranging from $10\,s^{-1}$ to $100\,s^{-1}$. Plastic deformation was thus still mainly controlled by thermally activated mechanisms during the present tests.

5.3. Level of mean dissipated energy per cycle $\langle \overline{W}_d \rangle$ level for the three materials

The mean dissipated energy per cycle $\langle \overline{W}_d \rangle$ versus stress amplitude curve normalized with respect to UTS, determined after 10^7 -cycles, was found very similar for the three materials (Fig. 17). That result proves, once again, that the dissipated energy came from plastic strain (glide of dislocations). The change in the slope of the curve (transition domain) is around 30% of UTS. In the case of copper, below this value (70 MPa), the surface of the specimens displayed slip bands. They were isolated and concentrated in few grains as observed for copper loaded at 56 MPa (24% of UTS) (Fig. 11b). Above this value, slip bands covered the surface of many grains (see Fig. 11b for copper loaded at 72 MPa (31% of UTS)). In the case of α-brass, below 30% of UTS (90 MPa), the early slip band vs stress amplitude curve (Fig. 16) showed that no slip band was observed at 10^7 cycles. About 8×10^7 cycles were necessary to observe the early slip bands. Above 30% of UTS, many slip bands were observed (see Fig. 15 at 134 MPa (44% of UTS)). In the case of α-iron, slip bands were detected at 30% of UTS (120 MPa) at 10^8 -cycles as illustrated in Fig. 13. From these results, it is not possible to correlate the appearance of slip bands to the sharp increase in dissipated energy in contrast with pioneer works on ultrasonic fatigue tests carried out by Mason and co-authors [32]. Interestingly, Mason and co-authors studied the relationship between internal friction and strain amplitude (push–pull loading) using ultrasonic device for OFHC copper, α-brass and α-iron (probably pure iron). The internal friction was found to be independent on strain amplitudes up to a critical value above which a sharp increase in internal friction was found. They associated the first region with anelastic mechanisms attributed to the bowing out of dislocations moving in a pinning network. The sharp increase in internal friction was associated with inelastic mechanisms due to the breaking of dislocations from the network pinning. That conclusion was supported by the observation of the early isolated slip bands on the surface of the specimens. More recently, from mean stress effect analysis, Mareau et al. [33] also associated the region of quasi-constant (or slight increase) in dissipated energy vs stress amplitude with anelastic mechanisms in the case of low-frequency fatigue test carried out on ferritic steels. In contrast, from EBSD and misorientation analysis, Munier [25] concluded that, in the case of ferritic steels, cyclically loaded at low frequency, inelastic rather than anelastic mechanisms occurred. In the present case, the observation of slip bands on the surface of the specimen suggests that inelastic mechanisms occurred at low stress amplitudes but probably only in few grains due to stress heterogeneities. Reasoning from macroscopic values such as the macroscopic stress amplitude and the dissipated energy is clearly not sufficient to deduce the occurrence of deformation and dissipative mechanisms at the local state. The transition between the slight to sharp rise in dissipated energy vs stress amplitude probably expressed an increase in numbers of grain displaying inelastic mechanisms, irreversible slip and early short cracks.

6. Conclusion

Very high cycle fatigue tests were conducted on three ductile single-phase polycrystalline materials (copper, α- brass and α-iron) using an ultrasonic technique at a loading frequency of 20 kHz. Slip markings and self-heating at the surface of the specimens were investigated to reveal microplastic mechanisms that occurred during the fatigue tests. The three materials were found to display similar behaviors:

- Their fatigue strength decreased by 10 MPa per decade above 10^7 cycles and no horizontal asymptote was detected.
- In the case of copper, α-brass and α-iron, the cracks leading to final fracture initiated at the surface of the specimens. In the case of copper, they grew intergranularly between one grain with slip markings and another grain without slip markings. In the case of α-iron, they grew transgranularly and intergranularly.
- The location of highest dissipated energy corresponded to the site of highest slip band activity, and the change in dissipation was accompanied by the development of slip bands.
- The level of dissipated energy per cycle was very similar for the three materials for ranges of stress amplitude below 30% of the static ultimate tensile stress.
- The transition between the slight to sharp rise in dissipated energy vs stress amplitude probably was attributed to an increase in the numbers of grain displaying inelastic mechanisms, irreversible slip and early short cracks.

However, the following differences between the three metals were noted:

- Both fcc materials exhibited a gradual increase in dissipated energy with increasing numbers of cycles at any stress amplitudes, while in bcc α-iron, a stable dissipative state was reached at least for stress amplitudes below 65% of the fatigue limit at 10^9 cycles.
- The morphology and location of slip markings were similar for both fcc materials but different for the bcc α-iron. In the case of copper and α-brass, the slip bands were straight, long, and parallel. They occurred in many grains, and some of them were transmitted through grain or twin boundaries. In the case of α-iron, they were wavy and crossed very few grains. These differences were related to the different anisotropic elastic coefficients and the difference in slip mode between fcc and bcc metals.

Acknowledgements

We would like to acknowledge the Agence Nationale de la Recherche France ANR-09-BLAN-0025-01 for the funding that

enabled this work to be carried out and Griset company for supplying copper and α-brass.

References

[1] Bathias C, Paris P. Gigacycle fatigue in mechanical practice. Dekker: M. CRC Press; 2004.
[2] Bathias C. Piezoelectric fatigue testing machines and devices. Int J Fatigue 2006;28:1438–45.
[3] Stanzl-Tschegg S. Very high cycle fatigue measuring techniques. Int J Fatigue 2014;60:2–17.
[4] Boulanger T, Chrysochoos A, Mabru C, Galtier A. Calorimetric analysis of dissipative and thermoelastic effects associated with the fatigue behavior of steels. Int J Fatigue 2004;26:221–9.
[5] Berthel B, Chrysochoos A, Wattrisse B, Galtier A. Infrared image processing for the calorimetric analysis of fatigue phenomena. Exp Mech 2008;48:79–90.
[6] Doudard C, Calloch S, Hild F, Roux S. Identification of heat source fields from infra-red thermography: determination of 'self-heating' in a dual-phase steel by using a dog bone sample. Mech Mater 2010;42:55–62.
[7] Maquin F, Pierron F. Heat dissipation measurements in low stress cyclic loading of metallic materials: from internal friction to micro-plasticity. Mech Mater 2009;41:928–42.
[8] Connesson N, Maquin F, Pierron F. Experimental energy balance during the first cycles of cyclically loaded specimens under the conventional yield stress. Exp Mech 2011;51:23–44.
[9] Mughrabi H. On multi-stage fatigue life diagram and the relevant life controlling mechanisms in ultra-high cycle fatigue. Fatigue Fract Eng Mater Struct 2002;25:755–64.
[10] Blanche A, Chrysochoos A, Ranc N, Favier V. Dissipation assessments during dynamic very high cycle fatigue tests. Exp Mech 2015;55:699–709.
[11] Phung NL, Favier V, Ranc N, Vales F, Mughrabi H. Very high cycle fatigue of copper: evolution, morphology and locations of surface slip markings. Int J Fatigue 2014;63:68–77.
[12] Phung NL, Favier V, Ranc N. Evaluating schmid criterion for predicting preferential locations of persistent slip markings obtained after very high cycle fatigue for polycrystalline pure copper. Int J Fatigue 2015;77:115–27.
[13] Wang C, Blanche A, Wagner D, Chrysochoos A, Bathias C. Dissipative and microstructural effects associated with fatigue crack initiation on an Armco iron. Int J Fatigue 2014;58:152–7.
[14] Wang C, Wagner D, Wang QY, Bathias C. Gigacycle fatigue initiation mechanism in Armco iron. Int J Fatigue 2012;45:91–7.
[15] Wang C, Wagner D, Wang Z, Bathias C. Very high cycle fatigue crack initiation mechanisms according 3D micron abreast pipes model of PSB on alpha-ferrite. Fatigue Fract Eng Mater Struct 2015;38:1–11.
[16] Germain P, Nguyen QS, Suquet P. Continuum thermomechanics. J Appl Mech-Trans Asme 1983;50:1010–20.
[17] Ranc N, Blanche A, Ryckelynck D, Chrysochoos A. POD preprocessing of IR thermal data to assess heat source distributions. Exp Mech 2015;55:725–39.
[18] Stanzl-Tschegg SE, Mughrabi H, Schönbauer B. Life-time and cyclic slip of copper in the VHCF-regime. Int J Fatigue 2007;29:2050–9.
[19] Stanzl-Tschegg SE, Schönbauer B. Mechanisms of strain localization, crack initiation and fracture of polycrystalline copper in the VHCF regime. Int J Fatigue 2010;32:886–93.
[20] Höppel HW, May L, Prell M, Göken M. Influence of grain size and precipitation state on the fatigue lives and deformation mechanisms of CP aluminium and AA6082 in the VHCF-regime. Int J Fatigue 2011;33:10–8.
[21] Cartensen JV, Mayer H. Very high cycle fatigue of thin walled tubes made from austenitic stainless steel. Fatigue Eng Mater Struct 2002;25:837–44.
[22] Mughrabi H, Wang Z. Deformation of polycrystals: mechanism and microstructures. In: Proceedings of second Riso intern sympos on metall mater sci.
[23] Zhao YH, Liao YY, Zhu YT. Influence of stacking fault energy on nanostructure under high pressure torsion. Mater Sci Eng, A 2005;410–411:188–93.
[24] Mughrabi H, Ackermann F, Herz K. Persistent slip bands in fatigued face-centered and body-centered cubic metals. In: Fatigue mechanisms, proceedings of an ASTM-NB5-NSF symposium, Kansas City.
[25] Munier R. Etude de la fatigue des aciers laminés à partir de l'auto-échauffement sous sollicitation cyclique: essais, observations, modélisation et influence de la pré-déformation plastique, PhD of Université de Bretagne, Brest; 2012.
[26] Hull D, Bacon DJ. Introduction to dislocations. Butterworth-Heinemann Publications – Elsevier; 2001.
[27] Sommer C, Mughrabi H, Lochner D. Influence of temperature and carbon content on the cyclic deformation and fatigue behaviour of alpha-iron. Part I: cyclic deformation and stress-behaviour. Acta Mater 1998;46:1527–36.
[28] Ledbetter HM, Reed RP. Elastic properties of metals and alloys, 1 iron, nickel, iron-nickel alloys. J Phys Chem 1973;2:531–617.
[29] Bathias C. There is no infinite fatigue life in metallic materials. Fatigue Fract Eng Mater Struct 1999;22:559–66.
[30] Mughrabi H, Herz K, Stark X. Cyclic deformation and fatigue behaviour of alpha-iron mono- and polycrystals. Int J Fract 1981;17:193–220.
[31] Campbell JD, Ferguson WG. The temperature and strain rate dependence of the shear strength of mild steel. Phil Mag 1970;81:63–82.
[32] MacDonald DE. Ultrasonic frequency metal fatigue: a review of the investigations of fatigue (fracture) and (structural) reliability. Eng Fract Mech 1976;8:17–29.
[33] Mareau C, Favier V, Weber B, Galtier A. Influence of the free surface and the mean stress on the heat dissipation in steels under cyclic loading. Int J Fatigue 2009;31:1407–12.